Electrorotation of Single Yeast Cells at Frequencies Between 100 Hz and 1.6 GHz

Ralph Hölzel
Institut für Biophysik der Freien Universität Berlin, 14195 Berlin, Germany

ABSTRACT The determination of complete electrorotation spectra of living cells has been made possible by the development of a quadrature generator and an electrode assembly that span the frequency range between 100 Hz and 1.6 GHz. Multiple spectra of single cells of the yeast *Saccharomyces cerevisiae* have been measured at different medium conductivities ranging from 0.7 to 550 μS cm^{-1}. A spherical four-shell model was applied that simulated the experimental data well and disclosed the four-layer structure of the cell envelope attributed to the plasma membrane, the periplasmic space, and a thick inner and a thin outer wall region. Below 10 kHz an additional rotation effect was found, which changed its direction depending on the ionic strength of the medium. This is supposed to be connected with properties of the cell surface and its close vicinity. From the four-shell simulation the following physical properties of cell compartments could be derived: specific capacitance of plasma membrane (0.76 μF cm^{-2}), periplasmic space (0.5 μF cm^{-2}), and outer wall region (0.1 μF cm^{-2}). The conductivity of cytoplasm, plasma membrane, and inner wall region were found to vary with medium ionic strength from 9 to 12 mS cm^{-1}, 5.8 nS cm^{-1} to ~50 nS cm^{-1}, and 6 μS cm^{-1} to 240 μS cm^{-1}, respectively.

INTRODUCTION

The structure and physiology of biological cells can be investigated by numerous well-established physical methods, e.g., patch clamping, impedance measurements, or electron microscopy, each having its own advantages and disadvantages. Complementary information can be furnished by electrorotation studies, which allow the noninvasive determination of electrical and geometrical properties of individual cells in vivo (Arnold and Zimmermann, 1982; Hölzel and Lamprecht, 1992; Huang et al., 1992; Fuhr and Hagedorn, 1996). Well-established quantitative theories allow a number of cell parameters to be extracted simultaneously from a single rotation spectrum (Fuhr, 1985; Wang et al., 1993). However, information yield has been limited so far for technical reasons, mainly because important parts of the spectra of intact cells are expected to lie at frequencies between 100 MHz and 1 GHz. In this frequency range amplitudes and phase relations of the applied fields are difficult to control, because cable and even electrode lengths become comparable with the fields' wavelengths.

In principle, not all parameters needed for the mathematical simulation can be deduced from a single spectrum, so some of them have to be measured differently or have to be taken from the literature. The number of independently accessible parameters restricts the complexity of the model used and thus its applicability to biological reality. This problem can be partly solved by measuring several electrorotation spectra under different environmental or biological conditions. However, this approach as well as literature values introduce additional errors due to biological variations between individuals.

In this study the routinely accessible frequency range for electrorotation is extended up to 1.6 GHz to gain complete electrorotation spectra. To limit the number of presupposed parameters, the medium conductivity is measured inside the rotation chamber and is varied without exchanging the cells themselves. Spectra are analyzed according to a four-shell spherical cell model.

MATERIALS AND METHODS

Yeast cells

Yeast cells of *Saccharomyces cerevisiae*, strain RXII, were grown in complete medium (1% yeast extract, 0.5% peptone, 2% glucose) at 35°C and harvested after 2 days during stationary phase. They were washed three times and resuspended in double-distilled water that had been prepared the day before. Medium conductivities were determined with a conductivity meter (LF Digi 550; WTW, Weilheim, Germany) and adjusted by addition of KCl. Cells were diluted ~1000-fold to give a density of 5–10 cells in the interelectrode space. All surfaces coming in contact with the cell suspension used in the experiment were thoroughly rinsed with double-distilled water and dried with an air jet.

Quadrature generator

To cover the extremely wide frequency range from 100 Hz to above 1 GHz, a special quadrature generator was developed in this laboratory. Four signals of equal amplitude and frequency, phase shifted by 90° each, are generated by a continuously tunable all-pass oscillator working up to 160 MHz (Hölzel, 1993a) and by five fixed frequency oscillators reaching 1.6 GHz (Fig. 1). For stable operation over such a wide frequency range, all radio frequency-carrying parts of the circuit are placed on epoxy glass copper-clad board in surface mount technology. All signal paths are transmission lines of 50 Ω impedance, i.e. coaxial cables or microstrip lines, to ascertain defined amplitudes and phases. Most signal conditioning and amplification is done by silicon or gallium arsenide MMICs (monolithic microwave integrated circuits). Great care was taken to produce signal

Received for publication 7 February 1997 and in final form 18 April 1997.
Address reprint requests to Dr. Ralph Hölzel, Institut für Biophysik, Freie Universität Berlin, Thielallee 63, 14195 Berlin, Germany. Tel.: 49-30-838-2682; Fax: 49-30-838-4323; E-mail: ralphbph@zedat.fu-berlin.de.

0006-3495/97/08/1103/07 $2.00

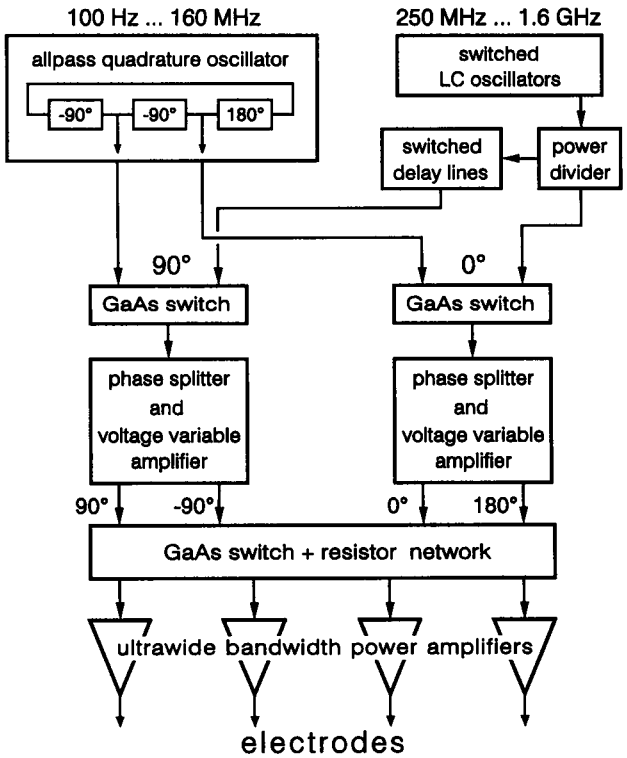

FIGURE 1 Principal structure of the electrorotation generator. Four signals of equal amplitude and frequency and 90° phase shift each are produced by a continuously tunable all-pass oscillator and five fixed frequency oscillators combined with delay lines.

pathways of identical length to minimize additional phase shifts, especially at high frequencies. At, e.g., 1 GHz, a difference in transmission line length of 1 mm corresponds to a phase error of 1.7°.

The continuously tunable oscillator is made of two identical first-order all-pass filters in series that exhibit a frequency-dependent phase shift and a frequency-independent amplification of around 1. The inverted output of the second stage is fed back into the first stage's input, thus leading to an oscillation exactly at that frequency, that is phase shifted by 90° by each all-pass. Amplification of both stages is automatically adjusted to 1 via a proportional integral regulator to compensate for additional frequency-dependent losses. Above some 150 MHz, tuning becomes less effective because of the finite group delay of ~0.5 ns of each stage. Therefore fixed oscillators are used at higher frequencies, followed by delay lines to accomplish the necessary phase shift. Phase splitters of variable amplification deliver the additional −90° and 180° signals. All four quadrature signals pass an electronic switch network to make not only electrorotation but also dielectrophoretic experiments possible, according to the method of Huang and Pethig (1991). The output amplifier stage can deliver up to 5.6 V_{pp} into a 50-Ω load at a voltage standing wave ratio (VSWR) of less than 2 up to 1 GHz, increasing somewhat at higher frequencies.

VSWR and amplification of each channel were checked and optimized by using an S-parameter test set combined with a lightwave component analyzer (HP 85046A and HP 8702A; Hewlett Packard, Palo Alto, CA). Phase angles were adjusted with a vector analyzer (ZPV with tuner ZPV-E2; Rohde and Schwarz, Munich, Germany). Frequencies were determined with a digital counter (UZ 2400; Grundig, Fürth, Germany). Harmonics were checked with a 100-MHz oscilloscope (PM 3266; Philips/Fluke, Kassel, Germany) up to 10 MHz; above that they were determined with a spectrum analyzer (762–2A; ST/Systron-Donner, Sunnyvale, CA) to be less than −30 dBc (i.e., 3% of the ground wave's amplitude).

Electrode chamber

The quadrature signals are fed to four electrodes in a square arrangement to produce the rotating electric field. Platinum wires of 0.1 mm diameter bent in a U-turn (Fig. 2) are used as electrodes to minimize disturbing dielectrophoretic effects (Hölzel, 1993b). Photolithographical techniques are not applied because they would introduce additional field inhomogeneities in the z direction and hence more disturbing cell movement by dielectrophoresis due to the limited thickness of the metal layer.

Because the rotation rate depends directly on the square of the electric field strength, the latter must be properly controlled. Therefore the electrode length, i.e., the distance between transmission line termination and electrode tip, should be as short as possible to minimize standing waves. On the other hand, long electrodes permit a large suspension volume, which helps to reduce the influence of contaminations on the suspending

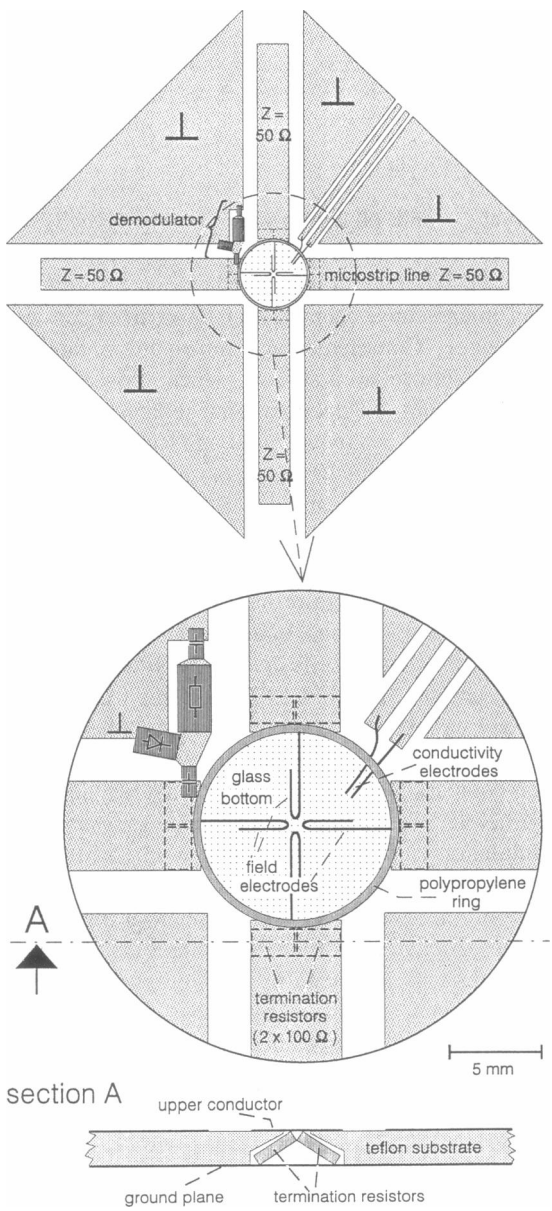

FIGURE 2 Schematic view of the electrode chamber. On a double-sided copper-clad Teflon board, transmission lines were shaped by photolithographical methods. Termination resistors are buried in the substrate for electrical and space reasons. The distance of opposite electrodes is 520 μm.

medium's conductivity. As a compromise, an electrode length of 4 mm is used. Electrodes are mounted on a double-sided copper-clad Teflon board (RT/duroid 5870; Rogers, Chandler, AZ) of 1.6-mm thickness. This material is ideally suited for microwave applications because of its low losses and well-defined dielectric properties. The microstrip lines of 4.5-mm width exhibit an impedance of 50 Ω and interfere much less with the rest of the electrode arrangement and microscope than coaxial cables. To minimize signal reflections and space requirements, termination of each transmission line is accomplished by two 100-Ω resistors in parallel, which are integrated into the board substrate beneath the ends of each stripline. For transmitted light microscopy, the board below the electrodes is replaced by a circular glass slide of 8-mm diameter that can easily be removed for cleaning or just be lowered for hanging drop experiments. Cell suspension and electrodes are enclosed by a polypropylene gasket of 1.1-mm height. Electrical connections are either soldered or made with conductive glue (RS, Stockport, England). For fixing and electrical insulation, paraffin wax (Fluka, Neu-Ulm, Germany) is used because of its low content of ionic contamination and to facilitate later rearrangements.

The signal amplitude is determined with a demodulator mounted as close to one of the electrodes as possible to minimize errors due to unavoidable reflections. To achieve both maximum sensitivity and minimal interference with the signal, a silicon Schottky diode of very low capacitance (0.35 pF) is used (BAT 62–03W; Siemens, Munich, Germany). This has been calibrated with a RF-mV-meter (RF 1000; Grundig) and a spectrum analyzer.

Suspension conductivities are commonly determined in a few milliliters before the rotation chamber is filled. That means subsequent contaminations cannot be considered, which are expected to be problematic at very low ionic strengths. This issue can be overcome by using two of the rotation electrodes for conductivity measurements within the rotation chamber itself (Arnold et al., 1987b). However, this is not possible here because of the parallel resistance of the termination resistors (100 Ω). For that reason, two extra platinum electrodes are mounted on the board and extend into the chamber volume. They are connected to the conductivity meter and have been calibrated with suspensions of known ionic strength, making it possible to monitor conductivity in the actual electrorotation volume in parallel with the experiment.

Field strength determination

To clarify the influence of parasitic effects like demodulator capacitance or electrode length, an equivalent circuit of the experimental setup after all four amplifier output stages was designed. Its frequency response was calculated with the help of an electronic circuit simulation program (PSpice 6.2; Microsim, Irvine, CA). Inductances and parallel capacitances of termination resistors and demodulator components were taken into account, as were the mutual capacitances between the electrodes, which had been measured with an impedance analyzer (HP 4192A; Hewlett Packard) at 13 MHz. Striplines and coaxial cables were modeled as ideal transmission lines, electrodes as lossy transmission lines. Because the electrodes are immersed in water, their geometrical length should be multiplied by the square root of the permittivity of water, i.e., by nearly 9. However, the finite water volume and the glass bottom reduce this factor significantly. By measuring the amplitudes at the amplifier output and at the chamber's demodulator, this factor could be estimated to amount to ~3.5. Mutual resistances between the electrodes were modeled as discrete resistors. The calculations revealed a resonance centered at 1.3 GHz, which is mainly a consequence of the effective electrode length. It leads to a voltage increase at the electrode tips by a factor of 2.2 at 1.0 GHz and 1.6 GHz, which decreases to 1.05 at 100 MHz. These factors do not vary with medium conductivity within the range applied in this study and were taken into account when the actual field strength was calculated.

The field geometry in the horizontal plane was calculated by using an equivalent resistor network model (Hölzel, 1993b). Subsequently it was corrected for in the z direction for the circular cross section of the electrode wires by applying a finite-element field analysis program (Elcut; TOR, St. Petersburg, Russia).

Rotation speed determination

Cells were observed under a microscope (BH2; Olympus, Hamburg, Germany) fitted with a video camera (CCD-G1E; Sony, Cologne, Germany) and a monitor (TC-1637DR; Panasonic, Hamburg, Germany). Rotation times were measured visually with a stopwatch. Spectra were determined at five points per frequency decade. This results in 36 points for a seven-decade spectrum, which could be measured in less than half an hour.

Evaluation of data

The derivation of cellular parameters from electrorotational data can be performed with the help of simple physical models that lead to mathematically exact solutions, e.g., for the cell membrane capacitance (Arnold et al., 1987a). However, taking into account the rather complex structure of a living cell, it is necessary to use more complicated sets of equations that can be solved only numerically. For this study a spherical double-shell model was applied based on the effective dipole moment method of Fuhr (1985) and a multishell smeared-out sphere model (Huang et al., 1992; Wang et al., 1993). The latter was used for the three-, four-, and five-shell simulations, because its mathematical expressions are relatively simple, even in the case of five concentric shells, and because its simplifications of the cell concern only the spherical symmetry and electrical homogeneity of each compartment. Theoretical curves were fitted to the experimental data with a sum-of-least-squares method.

RESULTS AND DISCUSSION

To find out whether induced dipoles are also the cause of electrorotation in the GHz range, which had been inaccessible so far, the correlation between applied field strength and rotation was determined at 1.0 and 1.6 GHz (Fig. 3). The double-logarithmic plot revealed a square dependence, as has already been shown at lower frequencies (Arnold and Zimmermann, 1982; Glaser et al., 1983; Hölzel and Lamprecht, 1987) with exponents 1.76 (r^2 = 0.992) and 1.96 (r^2 = 0.985) at 1.0 and 1.6 GHz, respectively.

Electrorotation experiments are commonly carried out at medium conductivities between 10 and 100 μS cm^{-1}. Only in recent years have higher conductive media also been used, giving additional information (Hölzel and Lamprecht,

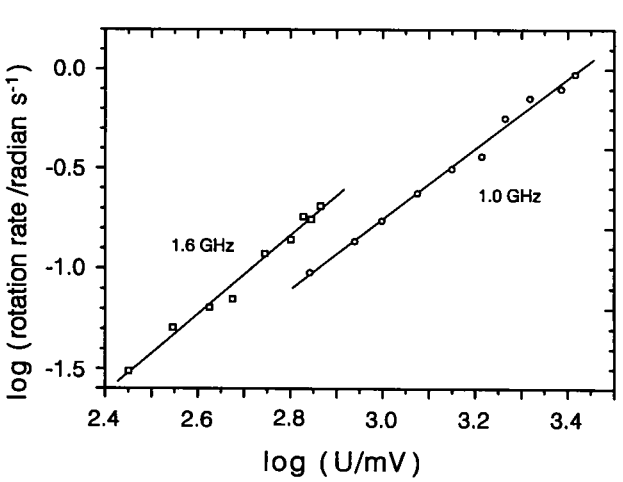

FIGURE 3 Dependence of rotation speed on the applied voltage at 1 GHz and 1.6 GHz in a double-logarithmic plot for two different cells at 6 μS cm^{-1} medium conductivity.

1992; Fuhr et al., 1994; Gimsa et al., 1996). Preliminary experiments on a murine B-lymphoblast cancer line, using the electrode configuration presented here (data not shown), have demonstrated the suitability of the setup, even at ionic strengths as high as that of a common culture medium like RPMA 1640 (~13 mS cm^{-1}). Surprisingly, very few experiments have been conducted below 10 μS cm^{-1} (Arnold et al., 1987b; Kaler and Johnston, 1985), although the conductivity of freshly distilled water is well below 1 μS cm^{-1}, increasing only slowly with time. Therefore yeast cells and electrodes were thoroughly washed with double-distilled water, achieving a final suspension conductivity of 0.7 μS cm^{-1} inside the rotation chamber. The corresponding spectrum (Fig. 4) was found to exhibit rather strong antifield rotation at very low frequencies, decreasing to 1 kHz and remaining constant up to 10 kHz. The zero crossing around 35 kHz is followed by a broad plateau up to 2.5 MHz and a distinct peak centered at 60 MHz.

Cellular properties can be extracted from a spectrum by a number of physical cell models, most of which are based on modeling the cell as a sphere consisting of several concentric shells. First the double-shell models according to Fuhr (1985) and Wang et al. (1993) were applied, assuming that the cell was surrounded by the cytoplasmic membrane and the cell wall. The two theories render nearly identical results (Fig. 4, *broken line*). The rotation below ~3 kHz presumably is not due to a Maxwell-Wagner relaxation and therefore is not covered by either of the theories. The plateau between 100 kHz and 2.5 MHz is considerably broader than can be simulated. The same holds true for the maximum at 60 MHz. In previous rotation experiments on *S. cerevisiae* (Kaler and Johnston, 1985; Arnold et al., 1986; Hölzel and Lamprecht, 1992; Huang et al., 1992), such a broadening was not discernible because of higher medium conductivity and limitations in accuracy or frequency range.

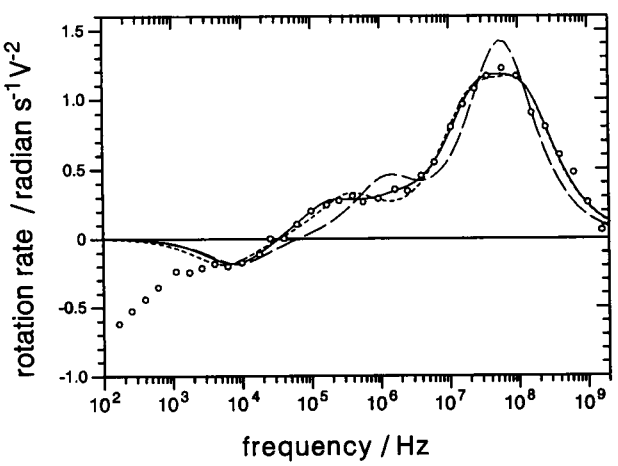

FIGURE 4 Electrorotation spectrum of *Saccharomyces cerevisiae* at 0.7 μS cm^{-1} medium conductivity (*open circles*). Curves represent least-square fits to the data above 3 kHz according to a double-, three-, and four-shell spherical cell model (*broken, dashed,* and *solid lines*, respectively).

The introduction of an additional shell made it possible to simulate either the high-frequency peak (Fig. 4, *dashed line*) or the plateau, still leaving a significant deviation in the remaining part of the spectrum. Only the extension to four shells (Fig. 4, *solid line*) rendered a good agreement. It is the first time that such a complex model has been applied to electrorotational data, and it might seem somewhat arbitrary to increase the complexity of a model just to fit the experimental data. However, the deviation from the simpler models significantly exceeds the experimental scatter. In addition, the model agrees very well with electron micrographs of *S. cerevisiae*, which reveal a three-layered structure outside the plasma membrane (Vitols et al., 1961; Moore et al., 1992; Mulholland et al., 1994). Next to the cytoplasmic membrane an electron-opaque layer is localized (usually referred to as the periplasmic space; Ganeva et al., 1995), followed by a less absorbing inner wall layer and the outer layer of high opacity. A least-squares fit based on a single layered cell envelope, but with two additional compartments inside the cell, which could be identified as the vacuole and its surrounding membrane, yielded unrealistic parameter values (data not shown). This demonstrates that the conditions of the applied model that reflect the biological system indeed constrain its correspondence to the experimental data, even for a model as complex as one that simulates the cell interior, four shells, and the surrounding medium.

Variation of external parameters like medium conductivity or toxin concentration can furnish additional information about cell structure and physiology. However, such variation has always been accomplished by modifying the medium or treating the cells outside the rotation chamber (Arnold et al., 1986, 1987a; Gimsa et al., 1991; Zhou et al., 1996). Depending on cell size, this makes the investigation of a single cell under different conditions very difficult or introduces additional errors due to biological variations between individual cells. For that reason, the medium conductivity inside the rotation chamber itself was altered by carefully sliding the coverslip aside and adding a few microliters of potassium chloride solution. After an initial increase the conductivity became constant ~15 min later, and rotation measurements were resumed.

The results for an individual cell at four distinct medium conductivities are shown in Fig. 5. Other measurements yielded very similar spectra, depending on medium ionic strength and cell size, but were conducted at less than four different conductivities. Obviously rotation above 20 MHz was nearly uneffected, as was expected from theory. Interestingly, below 3 kHz antifield rotation at 0.7 μS cm^{-1} changed to slow cofield rotation at 20 μS cm^{-1} and above and nearly ceased at 550 μS cm^{-1}. Such behavior could not be simulated by the four-shell model. Even the introduction of a fifth shell did not help. Some spectra taken around 3 μS cm^{-1} showed an increased antifield rotation with decreasing frequency, as in Fig. 5 *a*, whereas others exhibited nearly constant rotation below 3 kHz. The latter has also been reported by Arnold et al. (1986) for the same yeast strain at 10 μS cm^{-1}. Lamprecht and Mischel (1989) found

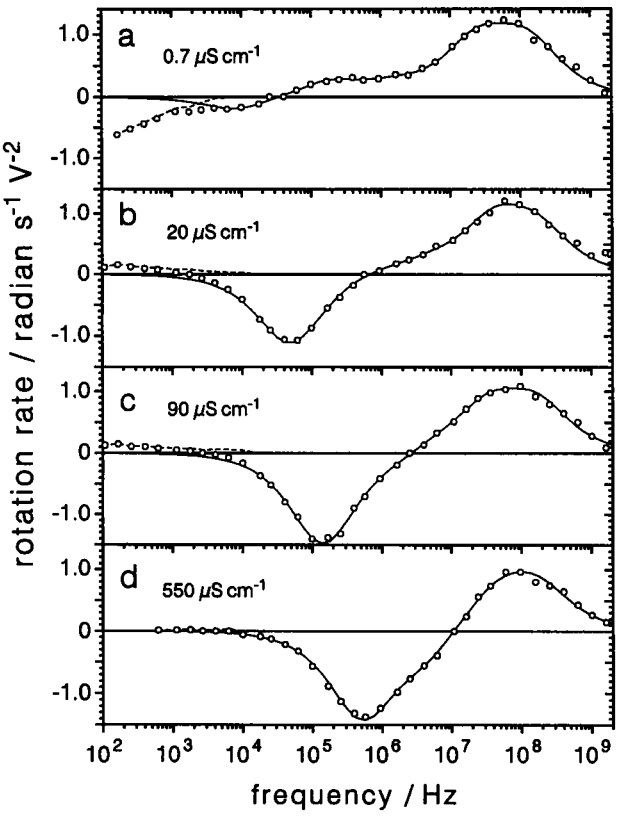

FIGURE 5 Electrorotation spectra of a single cell of *Saccharomyces cerevisiae* at four different medium conductivities. Curves represent least-square fits to the data above 3 kHz according to a four-shell spherical cell model. Below 20 kHz the difference between experiment and simulation is depicted by the dashed line.

a slow positive rotation at 8 μS cm^{-1}, which seems to contradict Arnold's and the present results, but might be explained by minor contaminations of their chamber, because they presumably determined the medium conductivity not inside the chamber, but in the stock suspension. Both their low-frequency observations and their zero crossing near 1 MHz coincide very well with the author's findings at 20 μS cm^{-1}. Yeast cells treated with ethanol (Arnold and Zimmermann, 1989), heavy metals (Arnold et al., 1986; Geier et al., 1987), ultrasound (Arnold et al., 1986), or heat (Hölzel and Lamprecht, 1987) exhibit an increased permeability of the plasma membrane and a still nearly unchanged negative rotation at low frequencies, whereas yeast protoplasts (Arnold and Zimmermann, 1989) show cofield rotation below 500 Hz. This demonstrates that low-frequency antifield rotation is connected with the cell wall. The increase in this effect with decreasing medium conductivity indicates that the counterion layer on the cell surface might cause this effect. The thickness of this layer, a measure of which is the Debye length, increases with the inverse square root of the ionic strength (Arnold et al., 1987b; Moore and Hummel, 1973). Estimating the layer's thickness as three Debye lengths and assuming a 1:1 salt leads to a thickness of 0.3 μm at 0.7 μS cm^{-1}, a value that exceeds even the cell wall thickness. In addition, what is conventionally thought of as the cell wall is surrounded by a highly hydrated capsular polysaccharide (Catley, 1991), which also might be the cause for this additional dispersion. The equations presented by Arnold et al. (1987b), based on their model of a dispersive particle in purely conductive medium, rendered reasonable results when applied to the present data at 0.7 μS cm^{-1}. However, to clarify the underlying phenomena, more detailed low-frequency experiments are necessary.

The application of a four-shell model turned out to be needed only at very low medium conductivities, where antifield rotation due to the cytoplasmic membrane decreased in both amplitude and characteristic frequency. At higher ionic strengths, cell wall phenomena were partly buried in this peak, so that the most detailed information about the wall could be established from low-conductivity experiments. When fitting the model to the data, one must keep in mind that each shell is defined by three physical parameters: its thickness or diameter, its electrical conductivity, and its permittivity. On the other hand, each shell adds one peak, which might be masked by another relaxation and which is completely defined by only two values, its height and its position. This means that even under optimal circumstances, an n-shell model, i.e., an object with $n + 1$ compartments plus the surrounding medium, renders $n + 1$ peaks based on at least $(n + 1) \cdot 3 + 2$ parameters, with external values like medium viscosity and electrical field strength excluded. The number of parameters can be slightly reduced by introducing relative values like the specific membrane capacitance. However, as many properties as possible should be determined independently.

To access the wall properties, geometrical dimensions were taken from electron micrographs of *S. cerevisiae* (Vitols et al., 1961; Moore et al., 1992; Mulholland et al., 1994). The resulting parameters are listed in Table 1. When the data are fitted, variation of the layer thickness d leads to a proportional change in permittivity ϵ and conductivity σ of that shell. This means that the model can deliver values for the ratios ϵ/d or σ/d, but only absolute values if one of these three parameters is known. Therefore the errors resulting from the electron micrographs directly influence the derived absolute wall properties. Permittivities of cell interior, cytoplasmic membrane, inner wall, and surrounding medium were taken from the literature (Asami et al., 1976; Pethig, 1979; Fuhr, 1985; Hölzel, 1990; Asami and Yonezawa, 1996). Cell sizes were determined microscopically. All other parameters were determined by a combined least-squares fit of single cell spectra at different medium conductivities, as shown in Fig. 5. Cellular permittivities were assumed to be independent of changes in medium conductivity. In the beginning the same was assumed for the conductivities of cell interior, periplasmic space, and outer wall layer. However, data measured at the lowest medium conductivity could not be simulated satisfyingly (data not shown), so they were also dealt with as variable parameters.

From impedance measurements above 1 mS cm^{-1}, it is known that the conductivity of the complete cell envelope

TABLE 1 Parameter values used for the least-squares curves of Fig. 5 according to a spherical four-shell cell model

	Thickness or radius	ϵ_r	Conductivity at medium conductivity (μS cm^{-1})			
			0.7	20	90	550
Interior	(3.0 μm)	(51)	9400	12000	12000	12000
Membrane	(3.5 nm)	(3.0)	0.0058	0.029	0.046	0.037
Periplasmic space	(25 nm)	14.4	11	41	41	41
Inner wall	(110 nm)	(60)	6.1	29	62	240
Outer wall	(50 nm)	5.9	100	200	200	200
Relative medium permittivity			(78)	(78)	(77.8)	(77)
Scaling factor			0.92	0.83	0.81	0.86

Numbers in parentheses are taken from the literature.

increases with medium conductivity (Asami et al., 1976; Asami and Yonezawa, 1996). From this study the same followed for the inner wall layer below 1 mS cm^{-1}. Extrapolation to higher ionic strengths in a double-logarithmic plot revealed a good agreement with the latest impedance data. The rather high permittivity of 60 takes into account the loose structure of this layer (Scherrer et al., 1974) with a high water content. The outer wall layer is supposed to be of finer porosity, being composed mainly of mannoproteins (Ganeva et al., 1995). This corresponds well to the permittivity of 5.9 found for this layer. The permittivity of the periplasmic space of 14.4 agrees well with the higher water content expected for this compartment. However, its thickness might be dependent on outside osmolarity and thus might not be constant, as was assumed for the simulation introducing additional systematic errors.

Cell membrane thickness was calculated at 3.5 nm. With an assumed relative permittivity of 3, this led to a specific capacitance of 0.76 μF cm^{-2}. Evaluating the dependence of the position of the antifield rotation maximum on medium conductivity according to the single-shell model of Arnold et al. (1987a) yielded 0.95 μF cm^{-2}. In a former rotation study at lower frequencies, in which the medium conductivity could not be determined in the chamber itself, a value of 1.1 μF cm^{-2} (Hölzel and Lamprecht, 1992) was found based on a double-shell model. This value has also been calculated from impedance measurements on yeasts up to 100 MHz by applying a single-shell model (Asami et al., 1976). In a recent paper (Asami and Yonezawa, 1996) the same group derives a value of 0.65 μF cm^{-2} from measurements up to 10 GHz by applying an improved theory. The remaining difference between this value and the present result of 0.76 μF cm^{-2} may be explained by folding and stretching of the membrane due to differing medium osmolarities that have been reported for mammalian cells (Wang et al., 1994). In addition, the calculations were based on different simplifications concerning the cell structure.

The electrical conductivity of the cell membrane is mainly reflected by the height of the antifield rotation peak, which is also influenced by the periplasmic space and the cell wall. Still, the simulation clearly showed an increase in membrane conductance from 5.8 nS cm^{-1} to ~50 nS cm^{-1} with increasing medium conductivity up to 100 μS cm^{-1}. Only a few data on the yeast's membrane conductance are available from the literature. Almost all are based on patch-clamp studies on yeast-protoplasts, which are difficult to perform because of the small size of yeast cells. Gustin et al. (1986) found voltage-dependent K^+ channels with a peak whole-cell conductance of some 40 pS cm^{-1}. From Bertl et al. (1995), 10-fold higher conductances follow, which are still at least one order of magnitude lower than the values of this study. However, mechanosensitive ion channels have been found in yeasts (Gustin et al., 1988), leading to a membrane conductivity of ~6 nS cm^{-1}. This conductivity strongly increased with the membrane's tension and is therefore limited in patch-clamp studies by the rupture of the protoplast's membrane, whereas in the experiments presented here the plasma membrane stayed intact because of the mechanical support by the cell wall. The osmotic pressure on the cell membrane can be estimated to at least an order of magnitude higher than in the patch-clamp studies. On the other hand, the channels' conductance might be dependent on the conductivity of its environment, which could be the reason for the observed increase in membrane conductance with increased medium conductivity below 100 μS cm^{-1}. Electrorotation studies varying medium osmolarity and ionic strength independently will help to clarify the function of yeast mechanosensitive channels.

The cytoplasmic conductivity was found to be independent of medium conductivity, except at very low ionic strengths amounting to 12 and 9.4 mS cm^{-1}, respectively. Impedance experiments render slightly lower values (Asami and Yonezawa, 1996), which might be caused by the differences between the underlying models in the vacuole and cell wall. A number of former impedance and rotation studies on yeast (Asami et al., 1976; Harris and Kell, 1983; Hölzel and Lamprecht, 1992; Huang et al., 1992; Zhou et al., 1996) yielded significantly lower values between 2 and 6 mS cm^{-1}. Interestingly, these values seem to increase with the upper frequency limit of the experiments. Up to some 10 MHz, the cell wall properties strongly influence the electrical response, whereas the cell's interior mainly determines the spectra around 100 MHz. Moreover, physical properties were assumed to be frequency independent, although, for example, the conductivity of free water increases in the GHz range (Pethig and Kell, 1987). Comparative studies on intact cells and protoplasts should clarify these differences.

In the course of the fitting procedure, a freely variable scaling factor was introduced to take into account uncertainties regarding field strength determination and friction effects neglected by the theory. The influence of friction with the supporting glass surface was ascertained by rotation measurements on sedimenting cells, leading to a reduction in rotation speed of 19% on the chamber bottom. This led to scaling factors ranging from 0.81 to 0.92, which presumably are a consequence of the exclusion of the roughness of the cell surface and its slight ellipsoidal shape (axial ratio 1:1.15:1) from the simulations.

A part of this work was supported by a grant of the Commission of the European Communities.

REFERENCES

Arnold, W. M., B. Geier, B. Wendt, and U. Zimmermann. 1986. The change in the electro-rotation of yeast cells effected by silver ions. *Biochim. Biophys. Acta.* 889:35–48.

Arnold, W. M., and J. S. Lacy. 1977. Permeability of the cell envelope and osmotic behavior in *Saccharomyces cerevisiae*. *J. Bacteriol.* 131: 564–571.

Arnold, W. M., R. K. Schmutzler, A. G. Schmutzler, H. van der Ven, S. Al-Hasani, D. Krebs, and U. Zimmermann. 1987a. Electro-rotation of mouse oocytes: single-cell measurements of zona-intact and zona-free cells and of the isolated zona pellucida. *Biochim. Biophys. Acta.* 905: 454–464.

Arnold, W. M., H. P. Schwan, and U. Zimmermann. 1987b. Surface conductance and other properties of latex particles measured by electrorotation. *J. Phys. Chem.* 91:5093–5098.

Arnold, W. M., and U. Zimmermann. 1982. Rotating-field-induced rotation and measurement of the membrane capacitance of single mesophyll cells of *Avena sativa*. *Z. Naturforsch.* 37c:908–915.

Arnold, W. M., and U. Zimmermann. 1989. Measurement of dielectric properties of single cells or other particles using direct observation of electro-rotation. *In* Proceedings of the 1st International Conference on Low Cost Experiments on Biophysics, Cairo University. UNESCO, New York. 1–13.

Asami, K., T. Hanai, and N. Koizumi. 1976. Dielectric properties of yeast cells. *J. Membr. Biol.* 28:169–180.

Asami, K., and T. Yonezawa. 1996. Dielectric behavior of wild-type yeast and vacuole-deficient mutant over a frequency range of 10 kHz to 10 GHz. *Biophys. J.* 71:2192–2200.

Bertl, A., J. A. Anderson, C. L. Slayman, and R. F. Gaber. 1995. Use of *Saccharomyces cerevisiae* for patch-clamp analysis of heterologous membrane proteins: characterization of Kat1, an inward-rectifying K^+ channel from *Arabidopsis thaliana*, and comparison with endogeneous yeast channels and carriers. *Proc. Natl. Acad. Sci. USA.* 92:2701–2705.

Catley, B. J. 1991. Isolation and analysis of cell walls. *In* Yeast, a Practical Approach. I. Campbell and J. H. Duffus, editors. IRL Press, Oxford. 163–183.

Fuhr, G. 1985. Über die Rotation dielektrischer Körper in rotierenden Feldern. Ph.D. dissertation. Humboldt University, Berlin.

Fuhr, G., H. Glasser, T. Müller, and T. Schnelle. 1994. Cell manipulation and cultivation under a.c. electric field influence in highly conductive culture media. *Biochim. Biophys. Acta.* 1201:353–360.

Fuhr, G., and R. Hagedorn. 1996. Cell electrorotation. *In* Electrical Manipulation of Cells. P. T. Lynch and M. R. Davey, editors. Chapman and Hall, New York. 37–70.

Ganeva, V., B. Galutzov, and J. Teissie. 1995. Electric field mediated loading of macromolecules in intact yeast cells is critically controlled at the wall level. *Biochim. Biophys. Acta.* 1240:229–236.

Geier, M. G., B. Wendt, W. M. Arnold, and U. Zimmermann. 1987. The effect of mercuric salts on the electro-rotation of yeast cells and comparison with a theoretical model. *Biochim. Biophys. Acta.* 900:45–55.

Gimsa, J., P. Marszalek, U. Loewe, and T. Y. Tsong. 1991. Dielectrophoresis and electrorotation of neurospora slime and murine myeloma cells. *Biophys. J.* 60:749–760.

Gimsa, J., T. Müller, T. Schnelle, and G. Fuhr. 1996. Dielectric spectroscopy of single human erythrocytes at physiological ionic strength: dispersion of the cytoplasm. *Biophys. J.* 71:495–506.

Glaser, R., G. Fuhr, and J. Gimsa. 1983. Rotation of erythrocytes, plant cells and protoplasts in an outside rotating electric field. *Stud. Biophys.* 96:11–20.

Gustin, M. C., B. Martinac, Y. Saimi, M. R. Culbertson, and C. Kung. 1986. Ion channels in yeast. *Science.* 233:1195–1197.

Gustin, M. C., X.-L. Zhou, B. Martinac, and C. Kung. 1988. A mechanosensitive ion channel in the yeast plasma membrane. *Science.* 242: 762–765.

Harris, C. M., and D. B. Kell. 1983. The radio-frequency dielectric properties of yeast cells measured with a rapid, automated, frequency-domain dielectric spectrometer. *Bioelectrochem. Bioenerg.* 11:15–28.

Huang, Y., R. Hölzel, R. Pethig, and X.-B. Wang. 1992. Differences in the AC electrodynamics of viable and non-viable yeast cells determined through combined dielectrophoresis and electrorotation studies. *Phys. Med. Biol.* 37:1499–1517.

Huang, Y., and R. Pethig. 1991. Electrode design for negative dielectrophoresis. *Meas. Sci. Technol.* 2:1142–1146.

Hölzel, R. 1990. Elektromagnetische Felder in der Umgebung lebender Zellen. Berlin-Verlag, Berlin.

Hölzel, R. 1993a. A simple wide-band sine wave quadrature oscillator. *IEEE Trans. Instrum. Meas.* 42:758–760.

Hölzel, R. 1993b. Electric field calculation for electrorotation electrodes. *J. Phys. D Appl. Phys.* 26:2112–2116.

Hölzel, R., and I. Lamprecht. 1987. Cellular spin resonance of yeast in a frequency range up to 140 MHz. *Z. Naturforsch.* 42c:1367–1369.

Hölzel, R., and I. Lamprecht. 1992. Dielectric properties of yeast cells as determined by electrorotation. *Biochim. Biophys. Acta.* 1104:195–200.

Kaler, K. V. I. S., and R. H. Johnston. 1985. Spinning response of yeast cells to rotating electric fields. *J. Biol. Phys.* 13:69–73.

Lamprecht, I., and M. Mischel. 1989. Cellular spin resonance. *In* Electroporation and Electrofusion in Cell Biology. E. Neumann, A. E. Sowers, and C. A. Jordan, editors. Plenum, New York. 23–35.

Moore, C. W., R. del Valle, J. McKoy, A. Pramanik, and R. E. Gordon. 1992. Lesions and preferential initial localization of [*S-methyl*-^{3}H]bleomycin A_2 on *Saccharomyces cerevisiae* cell walls and membranes. *Antimicrob. Agents Chemother.* 36:2497–2505.

Moore, W., and D. Hummel. 1973. Physikalische chemie. De Gruyter, Berlin.

Mulholland, J., D. Preuss, A. Moon, A. Wong, D. Drubin, and D. Botstein. 1994. Ultrastructure of the yeast actin cytoskeleton and its association with the plasma membrane. *J. Cell Biol.* 125:381–391.

Pethig, R. 1979. Dielectric and Electronic Properties of Biological Materials. John Wiley and Sons, New York.

Pethig, R., and D. B. Kell. 1987. The passive electrical properties of biological systems: their significance in physiology, biophysics and biotechnology. *Phys. Med. Biol.* 32:933–970.

Scherrer, R., L. Louden, and P. Gerhardt. 1974. Porosity of the yeast cell wall and membrane. *J. Bacteriol.* 118:534–540.

Vitols, E., R. J. North, and A. W. L. Linnane. 1961. Studies on the oxidative metabolism of *Saccharomyces cerevisiae*. *J. Biophys. Biochem. Cytol.* 9:689–699.

Wang, X.-B., Y. Huang, P. R. C. Gascoyne, F. F. Becker, R. Hölzel, and R. Pethig. 1994. Changes in Friend murine erythroleukaemia cell membranes during induced differentiation determined by electrorotation. *Biochim. Biophys. Acta.* 1193:330–344.

Wang, X.-B., Y. Huang, R. Hölzel, J. P. H. Burt, and R. Pethig. 1993. Theoretical and experimental investigations of the interdependence of the dielectric, dielectrophoretic and electrorotational behaviour of colloidal particles. *J. Phys. D Appl. Phys.* 26:312–322.

Zhou, X.-F., G. H. Markx, and R. Pethig. 1996. Effect of biocide concentration on electrorotation spectra of yeast cells. *Biochim. Biophys. Acta.* 1281:60–64.